MNRAS **000**, 1–5 (2018) Preprint 26 June 2018 Compiled using MNRAS LATEX style file v3.0

Hercules-Aquila and Virgo Clouds with Gaia DR2. Evidence for a common origin

Iulia T. Simion[1]⋆, Vasily Belokurov[2,3] and Sergey E. Koposov[2,4]
[1]*Key Laboratory for Research in Galaxies and Cosmology, Shanghai Astronomical Observatory, 80 Nandan Road, Shanghai 200030, China*
[2]*Institute of Astronomy, Madingley Rd, Cambridge, CB3 0HA*
[3]*Center for Computational Astrophysics, Flatiron Institute, 162 5th Avenue, New York, NY 10010, USA*
[4]*Department of Physics, McWilliams Center for Cosmology, Carnegie Mellon University, 5000 Forbes Avenue, Pittsburgh, PA 15213, USA*

Accepted XXX. Received YYY; in original form ZZZ

ABSTRACT
200 words for Letters.
No references should appear in the abstract.
Allowed maximum 5 pages in total.
..
..
..
..

Key words: keyword1 – keyword2 – keyword3

1 INTRODUCTION

How do you hide the evidence for a massive impact event that caused the extinction of most of the dinosaurs as well as 75% of all species on Earth? You bury it deep under the sea, covered with a layer of sediment taller than the Empire State Building (Hildebrand et al. 1991). Without the discovery of the giant Chicxulub crater, the meteorite impact hypothesis would remain a neat theory supported by striking but indirect evidence. A hypothesis of an ancient dramatic collision between the Milky Way and an unidentified massive dwarf galaxy was put forward by Deason et al. (2013) to explain a particular feature in the overall stellar halo density profile (Watkins et al. 2009; Deason et al. 2011). Most recently, through a study of a portion of the nearby stellar halo, Belokurov et al. (2018b) demonstrated that the great impactor must have collided with the young Milky Way on a nearly radial orbit, thus swamping the inner stellar halo with metal-rich material with orbital anisotropy (see Binney & Tremaine 2008) close to unity. Merger events like this tend to leave behind a battery of debris clouds and shells (see Amorisco 2015; Hendel & Johnston 2015), which - akin to the peak rings of impact craters (see e.g. Morgan et al. 2016) - if discovered could help to reconstruct the collision as well as pin down the properties of the progenitor (e.g Sanderson & Helmi 2013; Johnston 2016).

Before the Data Release 2 (Gaia Collaboration et al. 2018) of the ESA's Gaia mission (Gaia Collaboration et al. 2016), five large and diffuse cloud-like structures had been discovered in the Galaxy's halo. These include: the Virgo Over-Density (VOD, Vivas et al. 2001; Newberg et al. 2002; Duffau et al. 2006; Jurić et al. 2008; Bonaca et al. 2012), the Hercules-Aquila Cloud (HAC, Belokurov et al. 2007; Simion et al. 2014), the Trinagulum-Andromeda structure (Tri-And, Rocha-Pinto et al. 2004; Majewski et al. 2004; Deason et al. 2014), the Pisces Over-density (Sesar et al. 2007; Watkins et al. 2009; Nie et al. 2015) and the Eridanus-Phoenix over-density (Eri-Pho, Li et al. 2016). According to the most recent investigations, Tri-And likely comprises of Galactic disc stars kicked out of the plane in a recent interaction with a dwarf galaxy, probably the Sagittarius dSph (e.g. Price-Whelan et al. 2015; Bergemann et al. 2018; Hayes et al. 2018). Of the remaining four, the Pisces over-density clearly stands out as it reaches much larger Galacto-centric distances. On the other hand, the VOD, HAC and Eri-Pho structures occupy a very similar range of distances, between 10 and 20 kpc from the Galactic center. This lead Li et al. (2016) to suggest that these three Clouds could all be part of one merger event, a galaxy accreted onto the Milky Way on a polar orbit (see also Jurić et al. 2008).

As demonstrated by the recent re-interpretation of the Monoceros Ring (and the associated sub-structures) and the Tri-And, deciphering the nature of halo over-densities is often impossible without either high-resolution spectroscopy (e.g. Bergemann et al. 2018) or accurate astrometry (e.g. de Boer et al. 2018; Deason et al. 2018a). In this Letter, we look for clues to the formation of the Hercules-Aquila and Virgo Clouds using proper motions provided as part of the Gaia DR2. At our disposal are highly pure samples of members of each Cloud, namely the RR Lyrae stars that i) are co-spatial with HAC and VOD in 3-D and ii) that have their line-of-sight velocities measured. By complementing the publicly available 4-D data with the GDR2 proper motions, we build a large tracer set

⋆ E-mail:isimion@shao.ac.cn

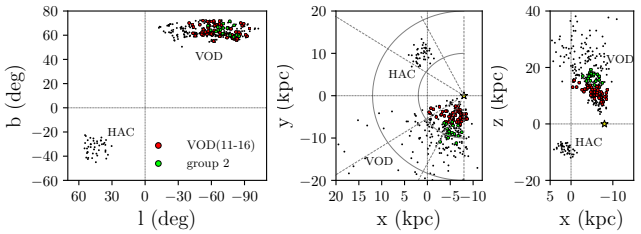

Figure 1. Spatial distribution of the RR Lyrae used in this work with 6-D phase space information, in Galactic coordinates (left panel) and projected onto the $x-y$ (middle) and $y-z$ (right) planes. With green we mark a 'high-significance' kinematical group (labeled 'group 2') identified by Vivas et al. (2016) and with red a sub-sample of the VOD RRL with similar galactocentric distances to the HAC sample, $11 < r_{GC}$ (kpc)< 16. The semi-circles are centred on the Sun's position and have radius of 10 and 20 kpc. The Sun (yellow star) is located at ($x_\odot$, $y_\odot$, $z_\odot$) = (-8,0,0) kpc and the Galactic centre at (0,0,0) kpc.

with complete 6-D phase space information and study the make-up of each structure using the orbital properties of the constituent stars.

2 DATA AND ANALYSIS

2.1 4-D RR Lyrae data

The Hercules-Aquila and Virgo Clouds are diffuse stellar over-densities in the inner stellar halo, located on the opposite sides of the Galaxy (see Figure 1). At high latitudes, these are detected as peaks in RR Lyrae number counts - curiously - at similar heliocentric distances, i.e. ∼17 kpc (HAC: Watkins et al. 2009; Simion et al. 2014) and ∼19 kpc (VOD: Vivas & Zinn 2006; Duffau et al. 2014; Vivas et al. 2016). Note that other tracers (e.g. BHBs, MSTO and K and M giants) have also been used to pin down the morphology of the Clouds (see e.g. Belokurov et al. 2007; Jurić et al. 2008; Sharma et al. 2010; Bonaca et al. 2012; Conroy et al. 2018). The RR Lyrae, however offer the clearest view of these halo sub-structures thanks to the associated accurate distances and minuscule Galactic foreground contamination. Therefore, in this work, we have focused on the two recently published samples of RR Lyrae towards the Clouds, where each star has a well-measured line-of-sight velocity.

- Simion et al. (2018) provide a table of 46 RRL with radial velocity measurements (45 observed with MDM and 1 from SDSS) with heliocentric distances between 15 and 18 kpc;
- Vivas et al. (2016) compiled a catalog of 412 RRL in the region of the sky covered by the VOD with distances between 4 and 75 kpc from the Sun with radial velocity measurements of stars from La Silla-QUEST, QUEST, CRTS and LINEAR.

2.2 From 4-D to 6-D. Velocity distributions

By cross-matching to the GDR2 data with an aperture of 2″, we have found Gaia counterparts to 44 HAC stars and 411 VOD. From the VOD sample, we remove 112 stars likely belonging to the Sgr stream as identified by (Vivas et al. 2016, , their group 1). The spatial distribution of the remaining stars (44 from Simion et al. 2018 and 299 from Vivas et al. 2016) with full 6-D phase space measurements is given in Figure 1, in Galactic coordinates in the left panel and in the x-y (x-z) Galactic plane in the middle (right) panel. We adopt a left-handed Galactic Cartesian coordinates with the Sun located at ($x_\odot$,$y_\odot$, $z_\odot$) = (-8,0,0) kpc, the x-axis positive in the direction of the Galactic center, y-axis oriented along the Galactic rotation and the z-axis directed towards the north Galactic pole. While Vivas et al. 2016 identify 6 significant kinematical groups in the VOD region (their table 5), only groups 1 (Sagittarius stream) and 2 (likely members of the VOD, with $< v_{GSR} > = 135$ km/s) contain more than 10 stars. We mark group 2 with green circles in Figure 1. We also mark with red circles the location of a group of stars selected to have galactocentric distances similar to the HAC sample, i.e. $11 < r_{GC}$(kpc)< 16 to facilitate a fair comparison of their velocities and orbits.

Figure 2 shows the spherical polar components of the velocities (radial v_r, azimuthal v_θ and polar v_ϕ) of stars in the HAC (top row) and VOD (bottom row) fields. Group 2 stars (green) can be seen clustering at $v_r = 135$ km/s (by design), while the stars at intermediate r_{GC} (red) seem to have a velocity distribution very similar to those in the HAC, shown in the top row. To estimate the uncertainty in each velocity component we propagate the measured proper motion and line-of-sight velocity errors using Monte-Carlo re-sampling, where we take into account the covariances between the measurements of the Right Ascension and Declination components of proper motion as provided in GDR2. We use the standard deviations of the resulting $\{v_r, v_\theta, v_\phi\}$ distributions as the upper limits of the velocity uncertainties; these are shown in Fig. 2.

As evident from the Figure, the velocity distributions are highly anisotropic, with the dispersion in the radial component dominating the tangential ones, especially in the HAC data. To describe the shape of the velocity distributions, we model each stellar sample as a single-component multi-variate Gaussian using the Extreme Deconvolution module implemented in astroML (Vanderplas et al. 2012). The resulting parameters and the associated uncertainties of the velocity ellipsoids are taken to be the median and the standard deviation values of 500 bootstrap re-sampling trials. The velocity ellipsoid shape can be summarized using the anisotropy parameter $\beta = 1-(\sigma_\theta^2+\sigma_\phi^2)/2\sigma_r^2$ (see Binney & Tremaine 2008). We find the HAC stars have radially biased orbits with $\beta = 0.91 \pm 0.03$ while for the whole of the VOD sample, $\beta = 0.74 \pm 0.04$. Note, however, that the two samples span very different ranges in Galactic l, b and distances. According to Belokurov et al. (2018b), the inner stellar halo can be viewed as a mixture of two debris components with distinct properties. Accordingly, we fit a model with two multivariate Gaussians to the VOD velocity data using Extreme Deconvolution (see Bovy et al. 2011). The VOD sample appears to be composed of roughly two thirds of stars with $\beta_1 = 0.96^{+0.02}_{-0.44}$ (marked in blue in Fig. 2) and a third with $\beta_2 = 0.44^{+0.45}_{-0.20}$ (magenta) in good agreement with the results for the local halo presented in Belokurov et al. (2018b). Using virial theorem, Myeong et al. (2018a) concluded that the radially anisotropic component of the stellar halo is also significantly flattened vertically. To test this hypothesis, we split the VOD sample into 3 groups according to their distance from the Galactic plane and show the behaviour of the azimuthal v_θ and radial v_r velocity distributions in Figure 3. Additionally, for each z slice we have calculated the fraction of Oosterhoff type I (Oo I) RR Lyrae, using equations 1 and 2 in Belokurov et al. (2018a) to explore the changes in the RRL mixture. In the 10<z/kpc<20 range, where the velocity anisotropy is the highest ($\beta = 0.84 \pm 0.03$) approaching the value in the HAC field, the Oo I type dominates (77%). In the same slice, 73% of the stars belong to the more squashed (or 'sausage' looking) velocity ellipsoid. The same behaviour but less accentuated can be noticed in the 0<z/kpc<10 slice where the anisotropy $\beta = 0.7 \pm 0.1$ is lower but the fraction of Oo I stars is somewhat lower at 57%. Further from the plane, at z>20 kpc, the velocity ellipsoid changes dramatically to almost isotropic with

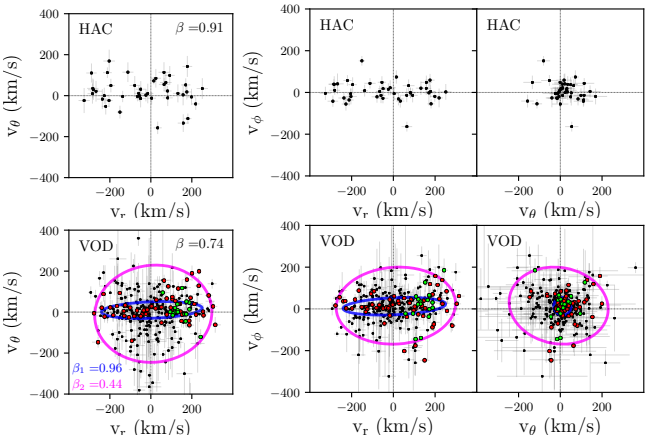

Figure 2. RRL velocity distribution in spherical polar coordinates (v_r, v_θ, v_ϕ are the radial, azimuthal and polar components respectively) of the HAC/VOD RR Lyrae, in the top/bottom panels. The error bars are the upper limit velocity uncertainties obtained through error propagation. The orbital anisotropy, is highly radial in the HAC field ($\beta = 0.91 \pm 0.03$) where the stars are most likely members of the Cloud and mildly radial in the VOD field ($\beta = 0.74 \pm 0.04$) where stars span a much wider range of distances (see Fig. 1). A mixture of two multivariate Gaussians was fitted to the VOD velocity ellipsoid: 62% of stars seem to belong to the $\beta_1 = 0.96^{+0.02}_{-0.44}$ (blue) component and 38% to the $\beta_2 = 0.44^{+0.45}_{-0.20}$ (magenta) component.

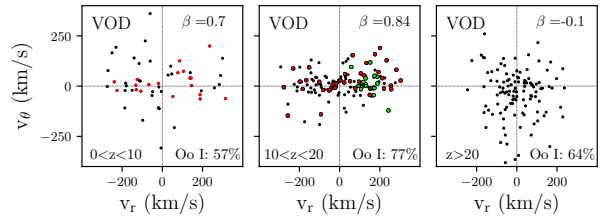

Figure 3. Radial and azimuthal velocity components in the VOD field, in three distance ranges above the Galactic plane. The fraction of RR Lyrae of Oosterhoff type I is reported in each panel, along with the orbital anisotropy β. Note the sub-sample of VOD RR Lyrae with $11 < r_{GC}$ (kpc)< 16 (marked in red) belong to the first two panels (z< 20 kpc) where $\beta \rightarrow 1$.

$\beta = -0.1 \pm 0.2$. Please note that in this particular z bin, the β value may still be affected by the presence of the Sagittarius stream. Group 2 and the stars sharing the same galactocentric distance range with the HAC, are all located at $z < 20$ kpc. Interestingly, the HAC counterparts in the VOD (red points) are all clearly part of the anisotropic component.

2.3 Orbital Properties

We use the 6-D measurements described above to initialise the RR Lyrae orbits in the HAC and VOD fields. The orbits are integrated using the galpy package (Bovy 2015) in the recommended Galactic potential model for the Milky Way, MWPotential2014 composed of a Miyamoto-Nagai disc, a bulge with a power-law density profile that is exponentially cut-off and a dark matter halo described by a NFW potential, with parameters given in Table 1 of Bovy (2015). The orbital properties, i.e. the peri- and apo-centric radii, eccentricity, and the maximal height above the disc plane, are shown in Figure 4. To compute the errors (not shown for VOD to simplify the figure) we integrate 500 orbits for each star where the initial conditions are re-sampled from the observations according to the associated uncertainties. The probability distributions of the ec-

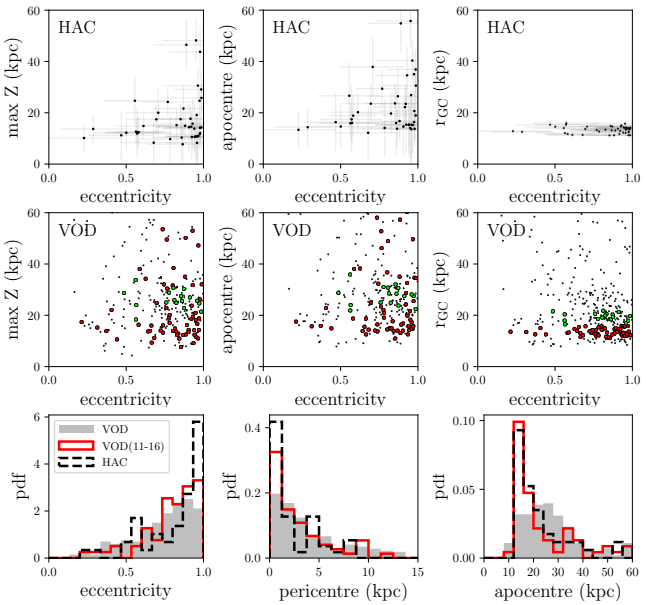

Figure 4. Properties of the RR Lyrae orbits in the HAC and VOD fields.

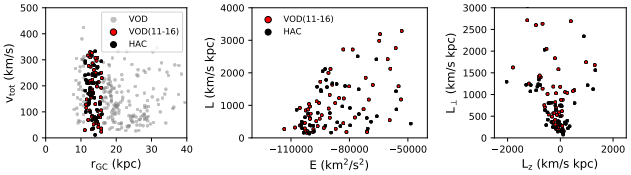

Figure 5. Total velocity versus galactocentric distance for VOD and HAC, showing in red the sub group VOD (11-16 kpc). Energy versus angular momentum and angular momentum only for stars with 11-16 kpc galactocentric distance. The energy here is the galpy energy minus the potential at infinity (will do what Sarah did too and see how it changes).

centricities, apo-centres and peri-centres are shown in the bottom row of the Figure. Note that the default Milky Way mass in galpy, $M_{vir} = 0.8 \times 10^{12} M_\odot$, is somewhat lower than suggested by recent measurements. We have checked however that the distributions of the orbital parameters displayed in Figure 4 are minimally affected if we increase the Galaxy's mass.

The stars in the HAC field typically travel as high as ∼15 kpc above the Galactic plane. The apo-centres bunch up around 15-20 kpc from the Galactic center, with a tail to higher values. The distribution of the peri-centric distances of the HAC stars peaks sharply around ∼1 kpc with most stars having their per-centers within 5 kpc from the Galactic center. This naturally implies highly eccentric orbits (with eccentricity close to 1) for the vast majority of the HAC stars. Compared to the HAC, the VOD stars explore broader range of apo-centres, with the distribution of the peri-centres much less strongly peaked. As a results, the typical eccentricity for a VOD star is around ∼0.8. Note however, that a sample of VOD stars comprised of Group 2 (shown in green) and stars that share instantaneous Galacto-centric distances with objects in the HAC field appears to have orbiral properties much closer to that of HAC. In particular, once the stars with similar distances are selected, the apo-centre and peri-center distance distributions in the two fields look very similar. The similarity of orbital properties of the HAC and VOD stars is emphasized in Figure 5. Here, we first show the current Galacto-centric radii and speeds of the stars in both fields

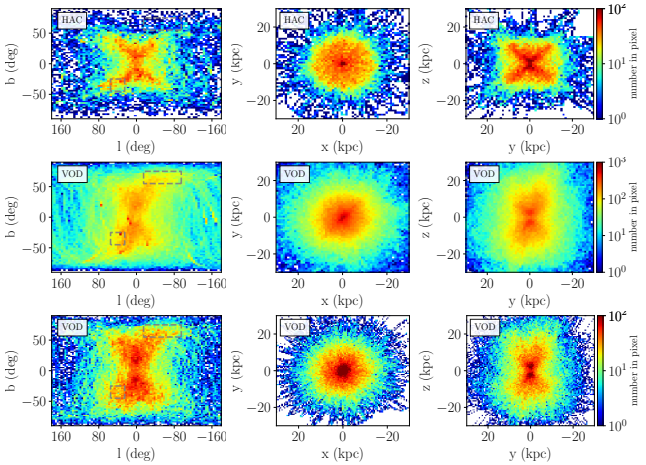

Figure 6. The backward orbit integration for HAC (top panels) and VOD (bottom panels) for 8 Gyrs look back time. We use $M_{vir} = 0.8 \times 10^{12} M_{\odot}$, the default galpy value . log(N) shown, notice the change in colour scale between top and bottom rows. The present day loci of HAC and VOD are marked with gray rectangles. The initial conditions of 44 stars with heliocentric distances between 15 and 18 kpc were used for the HAC backward orbit integration and of 299 stars with heliocentric distances between 4 and 75 kpc for the VOD orbit integration.

(left panel). Middle panel gives the distribution of total angular momentum as a function of energy for stars in the HAC (black) and stars in the VOD with matching distances ($11 < r_{GC}/\mathrm{kpc} < 16$, red). The bulk of the stellar debris in both fields are on high energy, low angular momentum orbits. Finally, the right panel of the Figure presents the distribution of the components of the angular momentum L_z and $L_\perp$. As evident from this panel, while stars in both HAC and VOD occupy highly radial orbits, both prograde and retrograde objects exist in both fields, with slight prevalence of the retrograde ones.

Figure 6 provides an alternative view of the orbital properties of the HAC and VOD stars. Here we have used the stellar 6-D phase-space measurements as initial conditions and integrated the orbits back in time for 8 Gyrs. The Figure shows the density of the test particle positions along each orbits for all orbits across the entire temporal range of the integration. The HAC stars occupy a slightly flattened (in the vertical direction) cross-like (in the y-z plane and its projection on the sky - l, b plane) structure with a density peak at the Galactic centre. Note that this particular appearance of the debris distribution is largely dictated by the limited initial conditions of the stars with available radial velocity measurements. The VOD stars typically move through very similar regions of the Galaxy (especially the distance-matched sub-sample) shown in the bottom row. While, overall, the match between the stellar debris distributions in Figure 6 is striking, the HAC and VOD stars studied here do not have identical orbital properties. For example, the VOD stars travel further above the Galactic disc, as exhibited by much rounder, or perhaps even vertically stretched, y-z distribution.

3 CONCLUSIONS

Using a sample of ~500 RR Lyrae with full 6-D phase space information, we have studied the orbital properties of the Hercules-Aquila and Virgo Clouds. Both Clouds appear dominated by stars on highly eccentric orbits. Assuming that the kinematics of each structure is well described by a single Gaussian, the orbital anisotropy of the HAC is $\beta = 0.91$ and for the VOD, $\beta = 0.74$. Note, however that the original criteria applied to the RR Lyrae stars to select targets for spectroscopic follow-up differ drastically between the HAC and the VOD datasets. The HAC sample covers a very limited region in the of l, b, D space, while the VOD dataset spans a wide range of longitudes, latitudes and heliocentric distances. It is therefore likely that the VOD dataset contains a mixture of several halo sub-structures (see Vivas et al. 2016, for a detailed discussion). For the entirety of the analysis described here, we made sure to cull the probable Sgr stream members. Additionally, we explore how the VOD's make-up changes with Galactic height and demonstrate that for $|z| < 20$ kpc, the VOD orbital anisotropy is $\beta \sim 0.84$, while above this threshold, it quickly changes to $\beta \sim 0$. We conclude therefore, that an assumption of a single Gaussian for the entire VOD sample is not appropriate. Modeling the kinematics of the VOD stars with a mixture of 2 multi-variate Gaussians, we show that two thirds of the VOD sample are the stars with $\beta = 0.96$, while the remainder has $\beta = 0.44$, in good agreement with the local measurement presented in Belokurov et al. (2018b).

As revealed by Gaia, the two structures are composed of stars on nearly radial orbits, with peaks in the eccentricity distribution at 0.9 (0.8) for the HAC (VOD). The distributions of the peri-centric and apo-centric distances also match: the stars in the Clouds turn around at 1 – 3 and 15 – 30 kpc. Not only the HAC and the VOD look alike kinematically, their orbital composition is in perfect agreement with the stellar halo properties as analysed locally by Belokurov et al. (2018b) and globally (out to 40 kpc) by Deason et al. (2018b). As these authors demonstrate, the inner halo is dominated by metal-rich debris from an old and massive accretion event. In particular, Belokurov et al. (2018b) use Cosmological simulations of Milky Way halo formation, to bracket the time of the merger - between 8 and 11 Gyr ago - and its mass, which they show to be in excess of $10^{10} M_{\odot}$. The tell-tale sign of this dramatic head-on collision is the particular shape of the corresponding stellar velocity ellipsoid, which is stretched so much in the radial direction compared to the tangential ones, that it resembles a sausage. An alternative view of this merger can be found in Myeong et al. (2018a), where the local stellar halo is mapped out in the action space. Here, the metal-rich stars are shown have extended radial action distribution in addition to a prominent spray of material on retrograde orbits. The high mass of the progenitor is evidenced not only by the metallicity distribution of its likely member or the numerical simulations of halo formation, but also by a sizeable number of Globular Clusters that could be attributed to the same event (see Myeong et al. 2018b).

Johnston et al. (2012) attempted to connect various clouds together.

ACKNOWLEDGEMENTS

The research leading to these results has received funding from the European Research Council under the European Union's Seventh Framework Programme (FP/2007-2013) / ERC Grant Agreement n. 308024.

REFERENCES

Amorisco N. C., 2015, MNRAS, 450, 575
Belokurov V., Deason A. J., Koposov S. E., Catelan M., Erkal D., Drake A. J., Evans N. W., 2018a, MNRAS, 477, 1472
Belokurov V., Erkal D., Evans N. W., Koposov S. E., Deason A. J., 2018b, MNRAS, 478, 611

Belokurov V., Evans N. W., Bell E. F., Irwin M. J. et al., 2007, ApJ, 657, L89
Bergemann M., Sesar B., Cohen J. G., Serenelli A. M. et al., 2018, Nature, 555, 334
Binney J., Tremaine S., 2008, Galactic Dynamics: Second Edition. Princeton University Press
Bonaca A., Jurić M., Ivezić Ž., Bizyaev D. et al., 2012, AJ, 143, 105
Bovy J., 2015, ApJS, 216, 29
Bovy J., Hogg D. W., Roweis S. T., 2011, Annals of Applied Statistics, 5
Conroy C., Bonaca A., Naidu R. P., Eisenstein D. J., Johnson B. D., Dotter A., Finkbeiner D. P., 2018, ArXiv e-prints
de Boer T. J. L., Belokurov V., Koposov S. E., 2018, MNRAS, 473, 647
Deason A. J., Belokurov V., Evans N. W., 2011, MNRAS, 416, 2903
Deason A. J., Belokurov V., Evans N. W., Johnston K. V., 2013, ApJ, 763, 113
Deason A. J., Belokurov V., Hamren K. M., Koposov S. E. et al., 2014, MNRAS, 444, 3975
Deason A. J., Belokurov V., Koposov S. E., 2018a, MNRAS, 473, 2428
Deason A. J., Belokurov V., Koposov S. E., Lancaster L., 2018b, ArXiv e-prints
Duffau S., Vivas A. K., Zinn R., Méndez R. A., Ruiz M. T., 2014, A&A, 566, A118
Duffau S., Zinn R., Vivas A. K., Carraro G., Méndez R. A., Winnick R., Gallart C., 2006, ApJ, 636, L97
Gaia Collaboration, Brown A. G. A., Vallenari A., Prusti T., de Bruijne J. H. J., Babusiaux C., Bailer-Jones C. A. L., 2018, ArXiv e-prints
Gaia Collaboration, Prusti T., de Bruijne J. H. J., Brown A. G. A. et al., 2016, A&A, 595, A1
Hayes C. R., Majewski S. R., Hasselquist S., Beaton R. L. et al., 2018, ApJ, 859, L8
Hendel D., Johnston K. V., 2015, MNRAS, 454, 2472
Hildebrand A. R., Penfield G. T., Kring D. A., Pilkington M., Camargo Z. A., Jacobsen S. B., Boynton W. V., 1991, Geology, 19, 867
Johnston K. V., 2016, in Astrophysics and Space Science Library, Vol. 420, Tidal Streams in the Local Group and Beyond, Newberg H. J., Carlin J. L., eds., p. 141
Johnston K. V., Sheffield A. A., Majewski S. R., Sharma S., Rocha-Pinto H. J., 2012, ApJ, 760, 95
Jurić M., Ivezić Ž., Brooks A., Lupton R. H. et al., 2008, ApJ, 673, 864
Li T. S., Balbinot E., Mondrik N., Marshall J. L. et al., 2016, ApJ, 817, 135
Majewski S. R., Ostheimer J. C., Rocha-Pinto H. J., Patterson R. J., Guhathakurta P., Reitzel D., 2004, ApJ, 615, 738
Morgan J. V., Gulick S. P. S., Bralower T., Chenot E. et al., 2016, Science, 354, 878
Myeong G. C., Evans N. W., Belokurov V., Sanders J. L., Koposov S. E., 2018a, ApJ, 856, L26
Myeong G. C., Evans N. W., Belokurov V., Sanders J. L., Koposov S. E., 2018b, ArXiv e-prints
Newberg H. J., Yanny B., Rockosi C., Grebel E. K. et al., 2002, ApJ, 569, 245
Nie J. D., Smith M. C., Belokurov V., Fan X. H. et al., 2015, ApJ, 810, 153
Price-Whelan A. M., Johnston K. V., Sheffield A. A., Laporte C. F. P., Sesar B., 2015, MNRAS, 452, 676
Rocha-Pinto H. J., Majewski S. R., Skrutskie M. F., Crane J. D., Patterson R. J., 2004, ApJ, 615, 732
Sanderson R. E., Helmi A., 2013, MNRAS, 435, 378
Sesar B., Ivezić Ž., Lupton R. H., Jurić M. et al., 2007, AJ, 134, 2236
Sharma S., Johnston K. V., Majewski S. R., Muñoz R. R., Carlberg J. K., Bullock J., 2010, ApJ, 722, 750
Simion I. T., Belokurov V., Irwin M., Koposov S. E., 2014, MNRAS, 440, 161
Simion I. T., Belokurov V., Koposov S. E., Sheffield A., Johnston K. V., 2018, MNRAS, 476, 3913
Vanderplas J., Connolly A., Ivezić Ž., Gray A., 2012, in Conference on Intelligent Data Understanding (CIDU), pp. 47 –54
Vivas A. K., Zinn R., 2006, AJ, 132, 714
Vivas A. K., Zinn R., Andrews P., Bailyn C. et al., 2001, ApJ, 554, L33
Vivas A. K., Zinn R., Farmer J., Duffau S., Ping Y., 2016, ApJ, 831, 165
Watkins L. L., Evans N. W., Belokurov V., Smith M. C. et al., 2009, MNRAS, 398, 1757

This paper has been typeset from a TEX/LATEX file prepared by the author.